Electronic Supplementary Information

Structure –property relationships in multifunctional thieno(bis)imide-based semiconductors with different sized and shaped N-alkyl ends

Manuela Melucci, [a],* Margherita Durso,[a] Cristian Bettini, [a,b] Massimo Gazzano, [a] Lucia Maini, [c] Stefano Toffanin, [d] Susanna Cavallini, [d] Massimiliano Cavallini, [d] Denis Gentili, [d] Viviana Biondo, [e] Gianluca Generali, [e] Federico Gallino, [f] Raffaella Capelli,[d] Michele Muccini [d,e]

a) Consiglio Nazionale delle Ricerche, Istituto per la Sintesi Organica e la Fotoreattività, (CNR-ISOF), via P. Gobetti 101, 40129 Bologna, Italy

b) MIST-ER Laboratory, via P. Gobetti 101, 40129 Bologna, Italy

c) Dipartimento di Chimica "G. Ciamician", Università di Bologna, Via F. Selmi 2, 40126 Bologna, Italy

d) Consiglio Nazionale delle Ricerche, Istituto per lo Studio dei Materiali Nanostrutturati (CNR-ISMN), via P. Gobetti 101, 40129 Bologna, Italy

e) E.T.C. s.r.l., via P. Gobetti 101, 40129 Bologna, Italy

f) SAES-GETTERS S. p. A., Viale Italia 77, 20020 Lainate - MI - Italy

Content:

1.0 Synthesis

General procedure for the synthesis of thienoimides 4a-g.

A solution of thieno[2,3-c]furan-4,6-dione (1.54 g, 1 mmol) **2** and alkylamine **3** (1.5 mmol) in 10 ml of toluene was refluxed for 48 h then the solvent was removed. The solid so obtained (made by a mixture of the regioisomers 2-(alkylcarbamoyl)thiophene-3-carboxylic acid and 3-(alkylcarbamoyl)thiophene-2-carboxylic acid), was washed with pentane and used for the following intramolecular dehydration without further purification. The isomers mixture (7.13 mmol) in thionyl chloride (140 ml) was refluxed for 5 h after that $SOCl_2$ was removed by distillation. The crude so obtained was purified by flash chromatography on silica gel to afford compounds **4a-g**.

5-Methyl-4H-thieno[2,3-c]pyrrole-4,6(5H)-dione, **4a**: Flash chromatography on silica gel, by using petroleum ether/CH_2Cl_2/AcOEt 80:10:10 as eluting phase afforded compound **4a** as a pale beige solid (Y = 91%).

EI-MS m/z 167 (M$^+$). ^{1}H NMR (CDCl$_3$, TMS/ppm) δ 7.74 (d, ^3J = 4.8 Hz, 1H), 7.30 (d, ^3J = 4.8 Hz, 1H), 3.11 (s, 3H). ^{13}C NMR (CDCl$_3$, TMS/ppm) δ 164.0, 162.8, 144.8, 140.9, 137.3, 121.1, 24.3.

5-Propyl-4H-thieno[2,3-c]pyrrole-4,6(5H)-dione, **4b**: Flash chromatography on silica gel, by using petroleum ether/AcOEt 90:10 as eluting phase afforded compound **4b** as a pale beige solid (Y = 92%).

EI-MS m/z 195 (M$^+$). ^{1}H NMR (CDCl$_3$, TMS/ppm) δ 7.74 (d, ^3J = 4.8 Hz, 1H), 7.30 (d, ^3J = 4.8 Hz, 1H), 3.57 (t, 2H), 1.67 (m, 2H), 0.94 (t, 3H). ^{13}C NMR (CDCl$_3$, TMS/ppm) δ 164.0, 162.8, 144.7, 140.9, 137.2, 121.1, 40.1, 22.1, 11.3.

5-Hexyl-4H-thieno[2,3-c]pyrrole-4,6(5H)-dione, **4d**: Flash chromatography on silica gel, by using petroleum ether/AcOEt 90:10 as eluting phase afforded compound **4d** as a yellow oil (Y > 95 %).

EI-MS m/z 237 (M$^+$). ^{1}H NMR (CDCl$_3$, TMS/ppm) δ 7.74 (d, ^3J = 4.8 Hz, 1H), 7.29 (d, ^3J = 4.8 Hz, 1H), 3.59 (t, 2H), 1.64 (m, 2H), 1.31 (m, 6H), 0.88 (t, 3H). ^{13}C NMR (CDCl$_3$, TMS/ppm) δ 164.0, 162.8, 144.7, 140.9, 137.2, 121.1, 38.5, 31.4, 28.8, 26.5, 22.5, 14.0.

5-Cyclohexyl-4H-thieno[2,3-c]pyrrole-4,6(5H)-dione, **4e**: Flash chromatography on silica gel, by using petroleum ether/AcOEt 95:5 as eluting phase afforded compound **4e** as a white solid (Y = 83 %).

EI-MS m/z 235 (M$^+$). ^{1}H NMR (CDCl$_3$, TMS/ppm) δ 7.71 (d, ^3J = 4.8 Hz, 1H), 7.27 (d, ^3J = 4.8 Hz, 1H), 3.99 (m, 1H), 2.13 (m, 2H), 1.77 (m, 2H), 1.74 (m, 3H), 1.33 (m, 3H). ^{13}C NMR (CDCl$_3$, TMS/ppm) δ 164.0, 162.8, 144.5, 140.9, 137.0, 121.0, 51.3, 30.1, 26.0, 25.0.

5-2-ethylhexyl -4H-thieno[2,3-c]pyrrole-4,6(5H)-dione, **4f***:* Flash chromatography on silica gel, by using petroleum ether/Et$_2$O 90:10 as eluting phase afforded compound **4f** as a yellow oil (Y = 86 %).

EI-MS m/z 265 (M$^+$). ^{1}H NMR (CDCl$_3$, TMS/ppm) δ 7.74 (d, ^3J = 4.8 Hz, 1H), 7.30 (d, ^3J = 4.8 Hz, 1H), 3.49 (d, ^3J = 7.2, 2H), 1.78 (m, 1H), 1.30 (m, 8H), 0.89 (m, 6H). ^{13}C NMR (CDCl$_3$, TMS/ppm) δ 164.5, 163.3, 144.9, 137.5, 137.3, 121.6, 121.1, 42.6, 38.5, 30.7, 28.7, 24.0, 23.2, 14.3, 10.7.

5-Octyl-4H-thieno[2,3-c]pyrrole-4,6(5H)-dione, **4g**: Flash chromatography on silica gel, by using petroleum ether/AcOEt 90:10 as eluting phase afforded compound **4g** as a yellow oil (Y = 67 %).

EI-MS m/z 265 (M$^+$). ^{1}H NMR (CDCl$_3$, TMS/ppm) δ 7.34 (d, ^3J = 4.8 Hz, 1H), 7.30 (d, ^3J = 4.8 Hz, 1H), 3.60 (t, 2H), 1.64 (m, 2H), 1.29 (m, 10H), 0.87 (t, 3H). ^{13}C NMR (CDCl$_3$, TMS/ppm) δ 164.0, 162.8, 144.7, 140.9, 137.2, 121.1, 38.5, 31.8, 29.2, 28.8, 26.8, 22.6, 14.1.

General procedure for the synthesis of brominated compounds 5a-g.

Thienoimide **4a-g** (1.41 mmol) was dissolved in trifluoroacetic acid (6 ml). After external ice cooling, 1 ml of concentrated sulfuric acid was introduced into the reactor. To this mixture solid N-bromosuccinimide (NBS, 1.37 mmol) was added in small portions over 6 h. After stirring overnight at room temperature, the brown solution was diluted with 10 ml of water and extracted with dichloromethane. The organic phase was dried over anhydrous magnesium sulfate and evaporated. The crude so obtained was then purified by flash chromatography on silica gel to afford compounds **5a-g**.

2-Bromo-5-methyl-4H-thieno[2,3-c]pyrrole-4,6(5H)-dione, **5a**: Purification by flash chromatography by using silica gel and petroleum ether/CH$_2$Cl$_2$/AcOEt = 80:10:10 as eluent afforded **5a** as a white solid in 67% yield.

EI-MS *m/z* 247 (M$^+$). ^{1}H NMR (CDCl$_3$, TMS/ppm) δ 7.31 (s, 1H), 3.09 (s, 3H). ^{13}C NMR (CDCl$_3$, TMS/ppm) δ 163.0, 162.0, 125.5, 123.8, 24.5.

2-Bromo-5-propyl-4H-thieno[2,3-c]pyrrole-4,6(5H)-dione, **5b**: Purification by flash chromatography by using silica gel and petroleum ether/AcOEt = 90:10 as eluent afforded **5b** as a white solid in 89% yield.

EI-MS *m/z* 275 (M$^+$). ^{1}H NMR (CDCl$_3$, TMS/ppm) δ 7.31 (s, 1H), 3.55 (t, 2H), 1.66 (m, 2H), 0.93 (t, 3H). ^{13}C NMR (CDCl$_3$, TMS/ppm) δ 163.0, 162.0, 143.8, 140.4, 125.4, 123.8, 40.2, 22.0, 11.2.

2-Bromo-5-hexyl-4H-thieno[2,3-c]pyrrole-4,6(5H)-dione, **5d**: Purification by flash chromatography by using silica gel and petroleum ether/AcOEt/CH$_2$Cl$_2$ = 90:5:5 as eluent afforded **5d** as yellow oil in 84% yield.

EI-MS *m/z* 317 (M⁺). ¹H NMR (CDCl₃, TMS/ppm) δ 7.30 (s, 1H), 3.57 (t, 2H), 1.62 (m, 2H), 1.30 (m, 6H), 0.88 (t, 3H). ¹³C NMR (CDCl₃, TMS/ppm) δ 163.0, 162.0, 143.9, 140.5, 125.4, 123.8, 38.7, 31.3, 28.7, 26.4, 22.5, 14.0.

2-Bromo-5-cyclohexyl-4H-thieno[2,3-c]pyrrole-4,6(5H)-dione, **5e**: Purification by flash chromatography by using silica gel and petroleum ether/AcOEt = 95:5 as eluent afforded **5e** as a yellow oil in 79% yield.

EI-MS *m/z* 315 (M⁺). ¹H NMR (CDCl₃, TMS/ppm) δ 7.28 (s, 1H), 3.97 (m, 1H), 2.11 (m, 2H), 1.85 (m, 2H), 1.70 (m, 3H), 1.30 (m, 3H). ¹³C NMR (CDCl₃, TMS/ppm) δ 163.0, 162.0, 143.7, 140.5, 125.1, 123.7, 51.6, 30.0, 26.0, 25.0.

2-Bromo-5-ethylhexyl-4H-thieno[2,3-c]pyrrole-4,6(5H)-dione, **5f**: Purification by flash chromatography by using silica gel and petroleum ether/AcOEt = 95:5 as eluent afforded **5f** as dark white solid in 78% yield.

EI-MS *m/z* 345 (M⁺). ¹H NMR (CDCl₃, TMS/ppm) δ 7.31 (s, 1H), 3.48 (d, ³*J* = 7.2 Hz, 2H), 1.76 (m, 1H), 1.28 (m, 8H), 0.89 (m, 6H). ¹³C NMR (CDCl₃, TMS/ppm) δ 163.2, 162.2, 143.8, 125.4, 124.0, 123.6, 42.5, 38.3, 30.4, 28.4, 23.7, 22.9, 14.0, 10.4.

2-Bromo-5-octyl-4H-thieno[2,3-c]pyrrole-4,6(5H)-dione, **5g**: Purification by flash chromatography by using silica gel and petroleum ether/AcOEt/CH₂Cl₂ 90:5:5 as eluent afforded **5g** as white solid in 88% yield.

EI-MS *m/z* 345 (M⁺). ¹H NMR (CDCl₃, TMS/ppm) δ 7.30 (s, 1H), 3.57 (t, 2H), 1.62 (m, 2H), 1.27 (m, 10H), 0.87 (t, 3H). ¹³C NMR (CDCl₃, TMS/ppm) δ 163.0, 162.0, 143.9, 140.5, 125.4, 123.8, 38.7, 31.8, 29.2, 29.1, 28.7, 26.8, 22.6, 14.1.
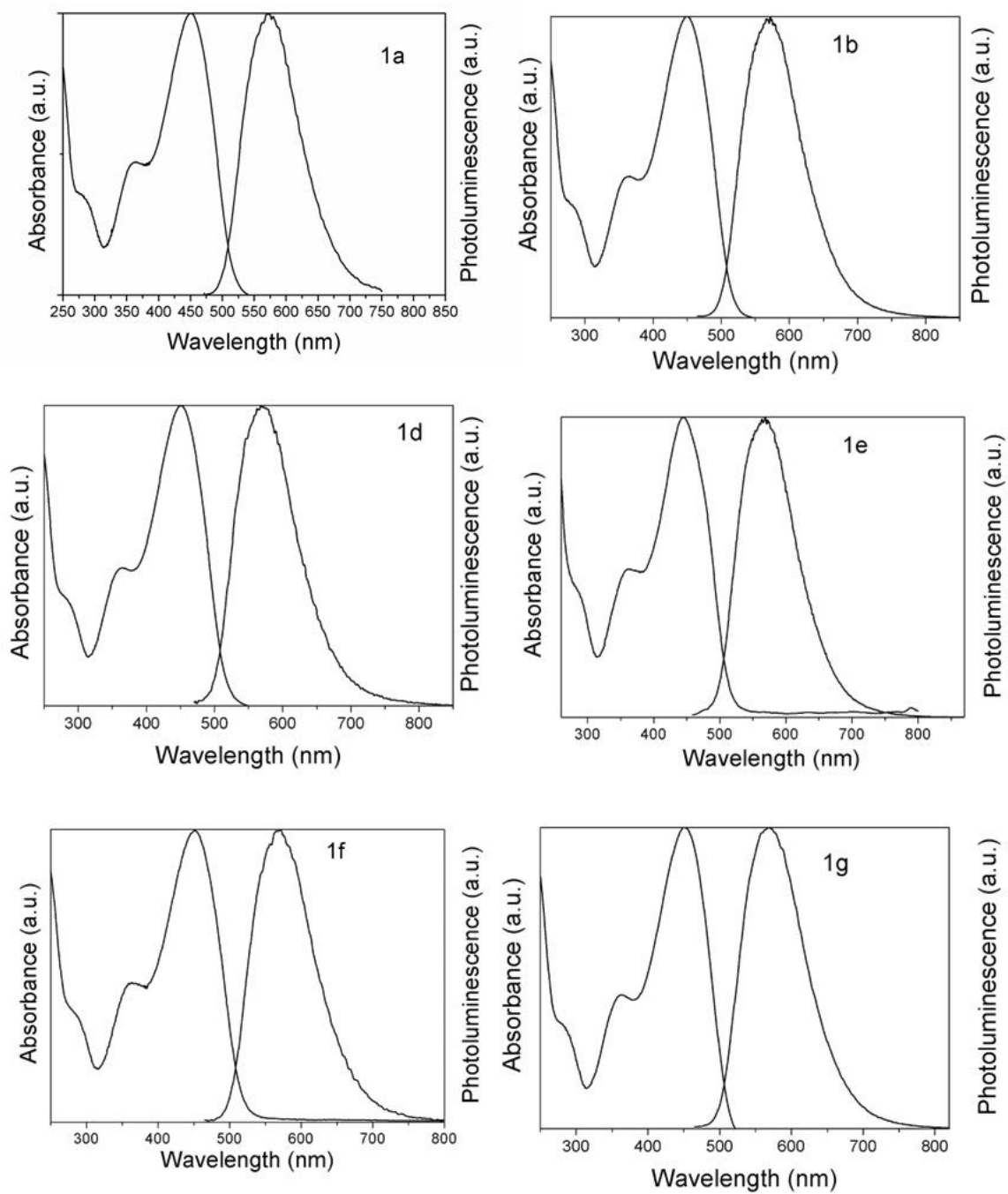
1.1 Optical properties in solution

Fig. S1.

Item	$\lambda_{max,}$ CH$_2$Cl$_2$ (nm)	$\lambda_{em,}$ CH$_2$Cl$_2$ (nm)
C1-NT4N (1a)	451	570
C3-NT4N (1b)	451	572
C4-NT4N (1c)	449	572
C6-NT4N (1d)	451	568
C6cyc-NT4N (1e)	444	568
C6br-NT4N (1f)	451	571
C8-NT4N (1g)	450	568

Table S1. Optical properties in dilute DCM solution
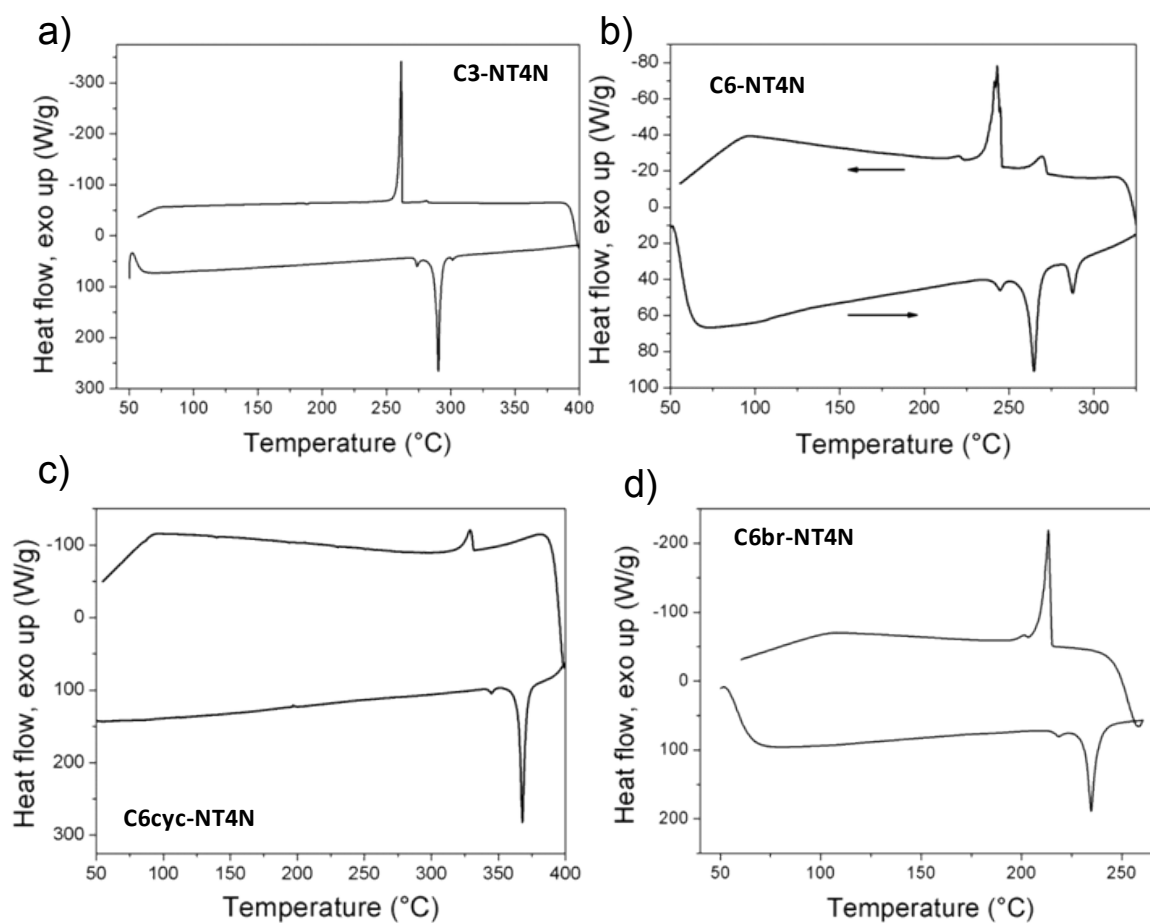
1.2 Differential Scanning Calorimetry

Fig. S2. DSC traces (second heating and cooling steps) at 20°C/min.

1.3 Thin deposits and thermal behaviour

Compound C1-NT4N, **1a** formed small crystallites with irregular shape whose mean size was below 2 μm (therefore at the limits of the optical resolution). The crystallites exhibited a slight birefringence disappearing at about 350 °C in air (and at 430 °C when the thin deposit is heated in between two glass slides).

Compound C3-NT4N, **1b** formed micrometer sized rod-like crystals. POM showed the typical behaviour of optical anisotropic substances, *i.e.* the crystals appeared coloured under crossed

polars. By rotating the crystal orientation vs. the polarised light, the crystals extinguished in four positions at intervals of 90°. The evidence of light extinguishment at the same orientations in all crystals indicated that all domains have the same orientation. No correlation among the orientation of different crystals was observed. By heating above 260 °C, **1b** became a smectic liquid crystal. At this temperature the size of birefringent domains increased up to few tens μm and then melted at about 300 °C. At this temperature thin deposit dewetted forming a homogeneous distribution of droplets. The liquid droplets have the typical behaviour of smectic LC. When cooling down below LC transition the droplets form large platelet like, highly birefringent crystals.

Compound C4-NT4N, **1c,** similarly to C3-NT4N, formed rod-like crystals whose size range from few tens μm to few hundred μm with the same behaviour observed at POM. Each crystal exhibited birefringence that extinguished by crossing the polarisers. A liquid crystal transition occured at about 270°C to give a smectic phase. Finally, the transition to isotropic phase occured at 290 °C. When cooled down to room temperature the droplets form large, birefrangent, crystals.

Compound C6-NT4N formed a continuous film on the surface whose thickness increases from the centre of thin deposit to the boundaries. The film exhibited birefringence without extinguishing at any direction under POM. Furthermore in the centre of the deposit birefrangent fiber-like crystals were often observed. Noticeably AFM showed that the fibers derived from the aggregation of small platelet-like crystals. At 245°C C6-NT4N became a liquid crystal and finally melted at about 300°C. At this temperature thin deposit dewetted forming a homogeneous distribution of droplets. When cooled down to room temperature the droplets formed large, birefringent, crystals.

Compound C6cyc-NT4N, **1e** formed rod-like crystals whose size ranged from few tens μm to few hundred μm. The crystals exhibited birefringence and extinguished when oriented parallel or perpendicular to the polariser. **1e** decomposed at about 400°C in air.

Compound C6br-NT4N, **1f** formed small crystals of irregular shape whose typical size ranged between 2 μm and 10 μm. At 210 °C it formed a smetic liquid crystal. At this temperature the size of birefrangent domains increased untill few tens μm. the transition to isotropic liquid occurred at 240°C. When cooled at room temperature the droplets form large platelet like, birefrangent crystals.
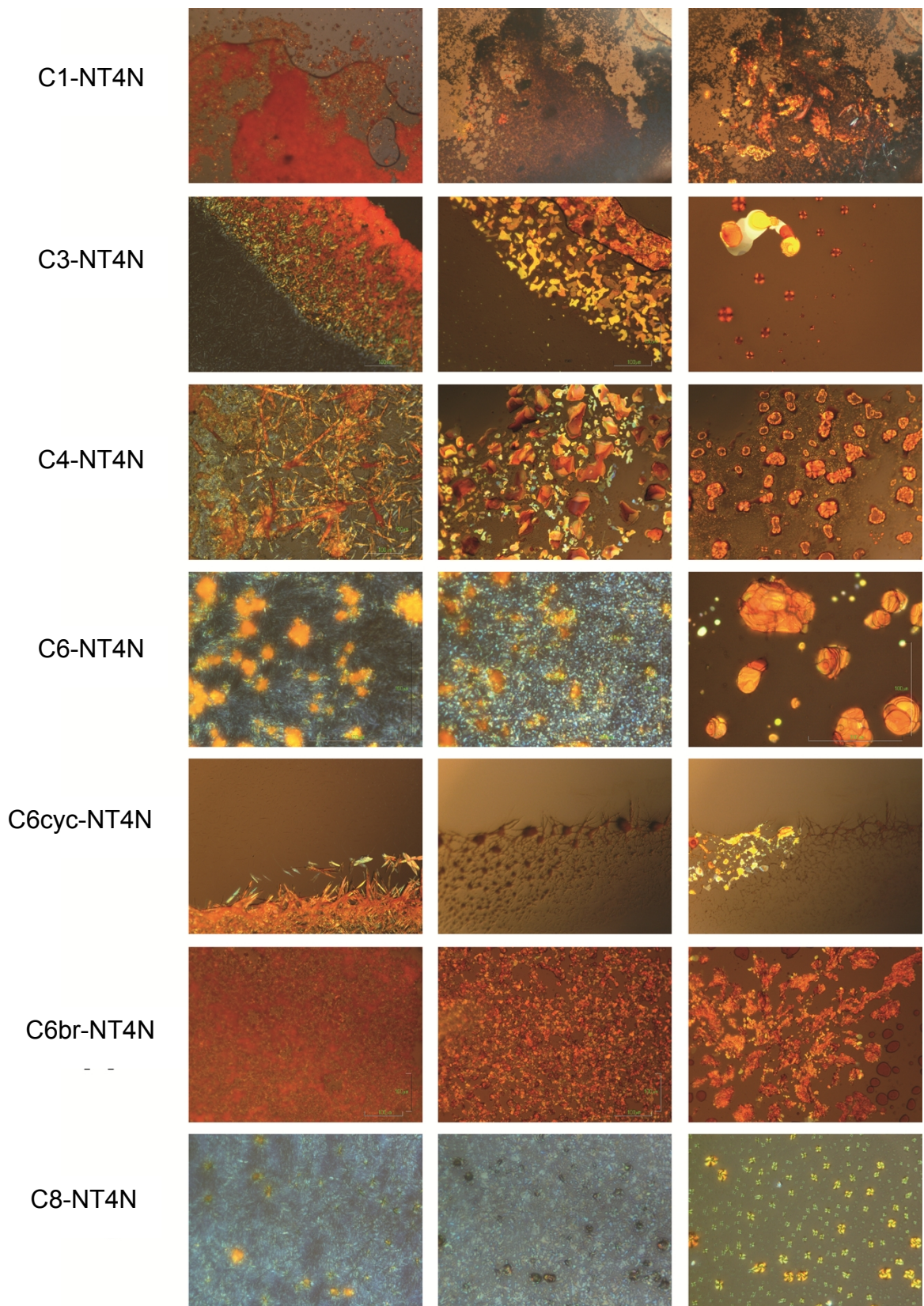
C1-NT4N

C3-NT4N

C4-NT4N

C6-NT4N

C6cyc-NT4N

C6br-NT4N
- -

C8-NT4N

Fig. S3.
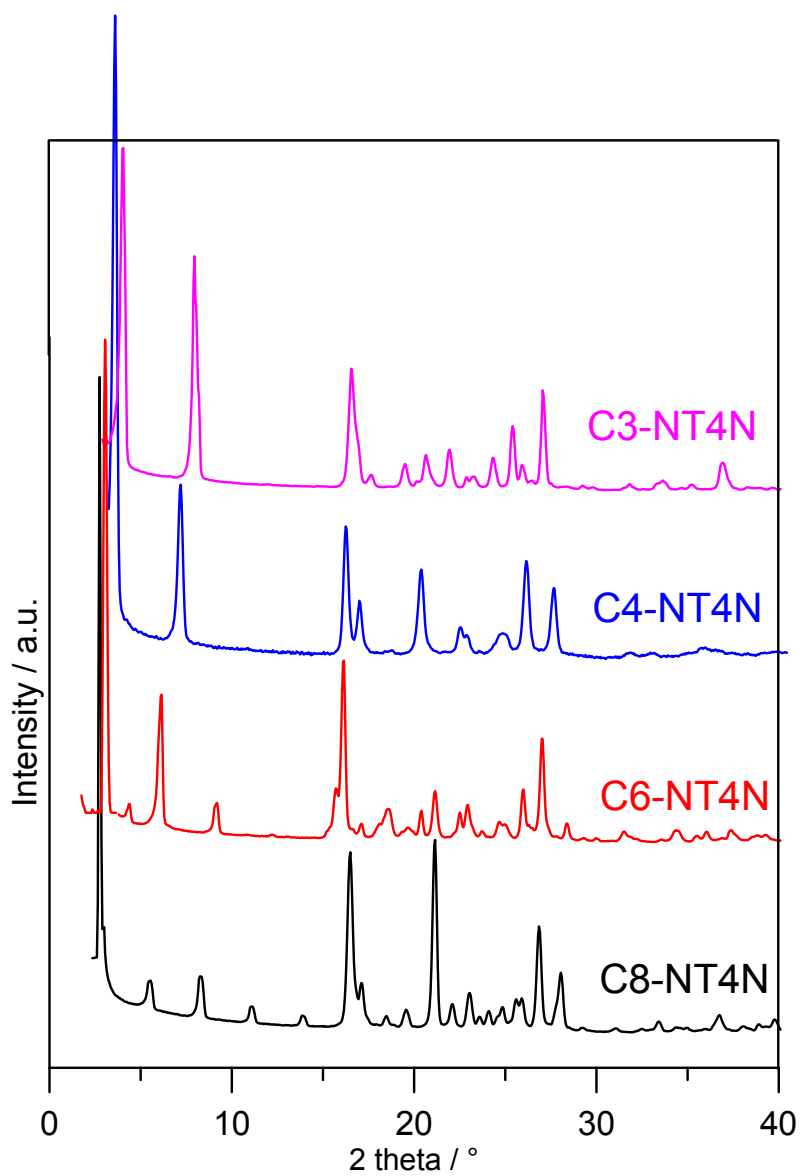
1.4 X-ray diffraction

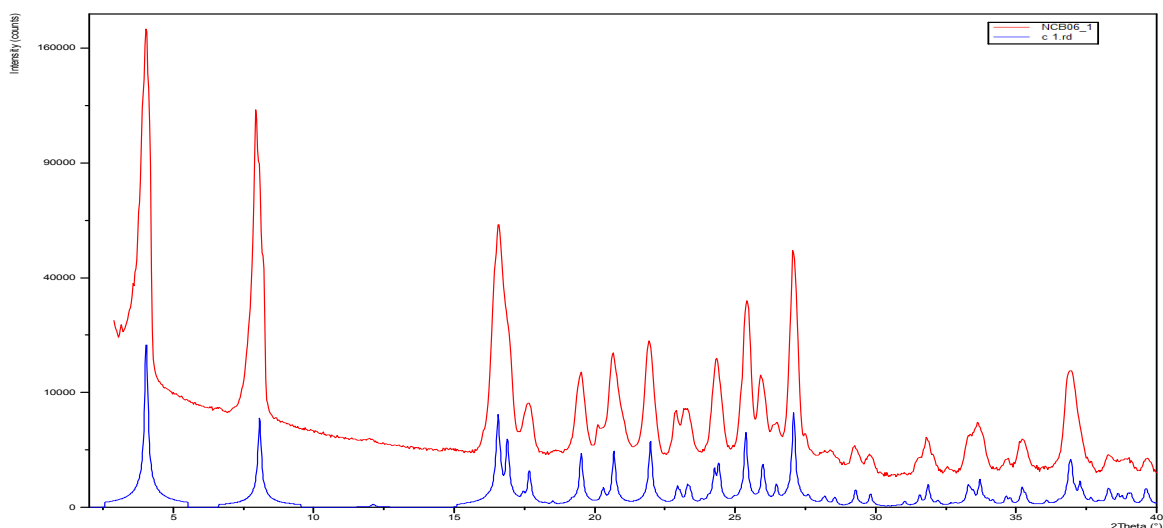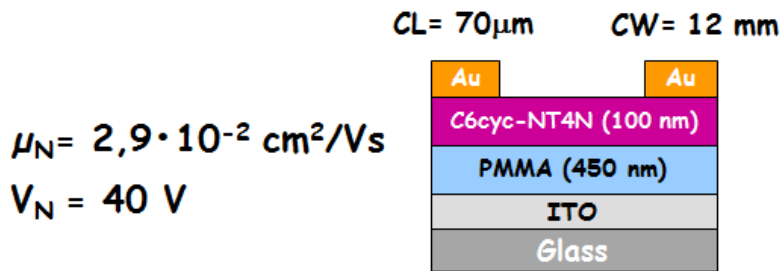**Fig. S4.** XRD patterns of compounds C3, C4, C6, C8-NT4N (powders).

Fig. S5. Comparison between experimental (red line) and calculated (blue) profile for compound C3-NT3N.

Single crystal X-ray diffraction (SC XRD): Crystal data for C3-NT4N were collected on an Oxford Xcalibur S with MoKα radiation, λ= 0.71073Å, monochromator graphite at room temperature. Crystal data and structure refinement parameters are summarized for C3-NT4N in the Table below. SHELX97[1] was used for the structure solution and refinement based on F^2. Non-hydrogen atoms were refined anisotropically. The MERCURY [2] software package was used for the graphical representation of the structure and powder pattern calculation.[3]
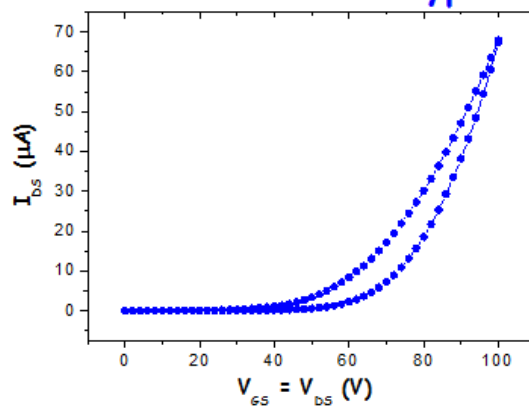
Formula	$C_{26} H_{20} N_2 O_4 S_4$
M, g mol^{-1}	552.68
Crystal system	Monoclinic
Space Group	C2/c
a, Å	7.4707(8)
b, Å	7.7479(6)
c, Å	43.819(6)
β, deg	91.54(1)
V, Å³	2535.4(5)
Z	4
Calculated density g cm^{-3}	1.448
$R_1{}^a$, $wR_2{}^b$	0.0787, 0.1785
GOF on F^2	1.167

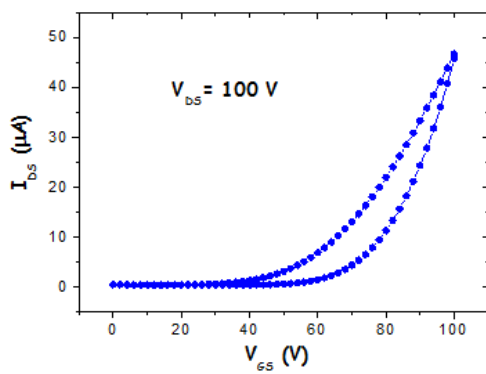a) R1 = $\sum(|F_o| - |F_c|)/\sum(|F_o|)$ and b) wR2 = $[\sum\{w(F_o{}^2 - F_c{}^2)^2\}/\sum\{w(F_o{}^2)^2\}]^{1/2}$

12

1.5 Electrical properties of compound C6cyc-NT4N

CL= 70μm   CW= 12 mm

| Au | | Au |

C6cyc-NT4N (100 nm)

PMMA (450 nm)

ITO

Glass

$\mu_N = 2{,}9 \cdot 10^{-2} \ cm^2/Vs$

$V_N = 40 \ V$

Locus curve N type

I_{DS} (μA)

$V_{GS} = V_{DS}$ (V)

Saturation Transfer curve N type

I_{DS} (μA)

$V_{DS} = 100 \ V$

V_{GS} (V)

Multiple Output curve N type

$V_{GS} = 0, 20, 40, 60, 80, 100 \ V$
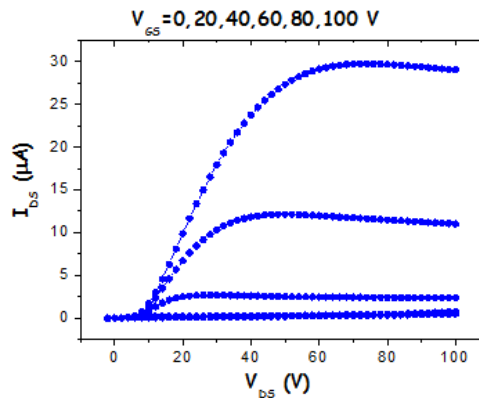
I_{DS} (μA)

V_{DS} (V)

Fig. S6.

13

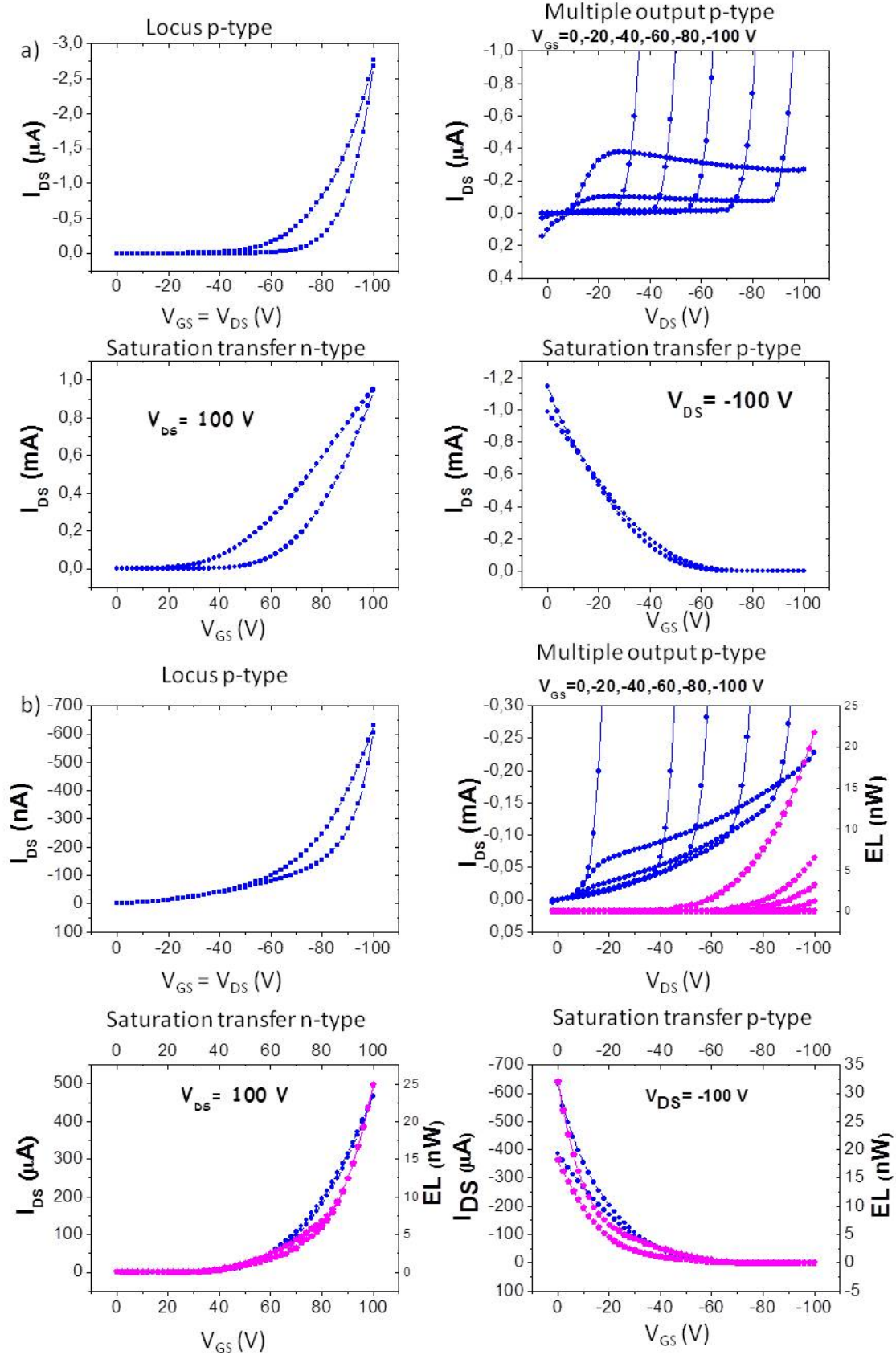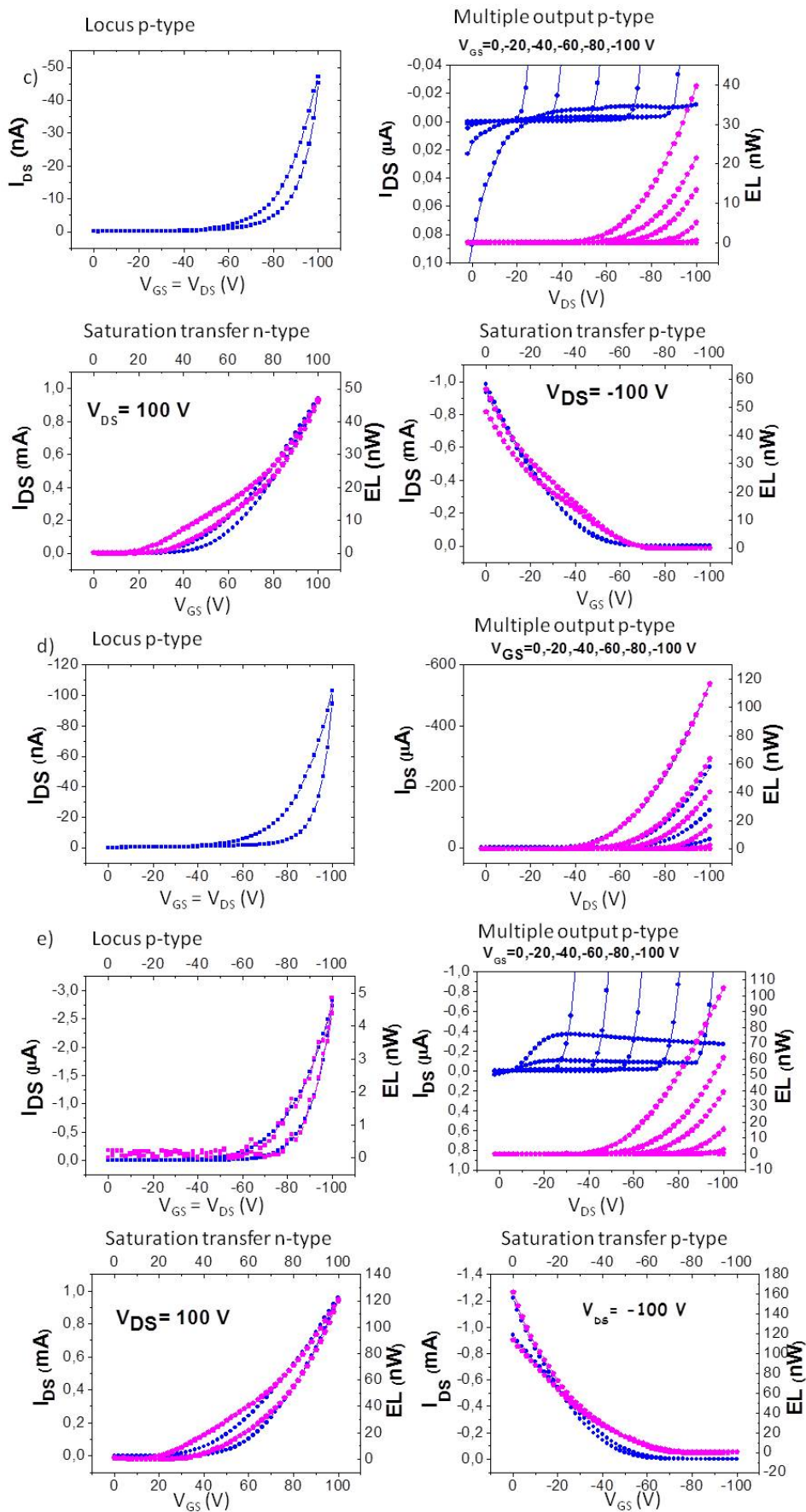## 1.6 Locus p-type, multiple output p-type and saturation transfer curves

Fig. S7. Electrical responses for compounds C1-NT4N (a), C3-NT4N (b), C4-NT4N (c), C6-NT4N (d) and C8-NT4N (e).

1.7 Locus n-type, multiple output n-type and saturation transfer curves
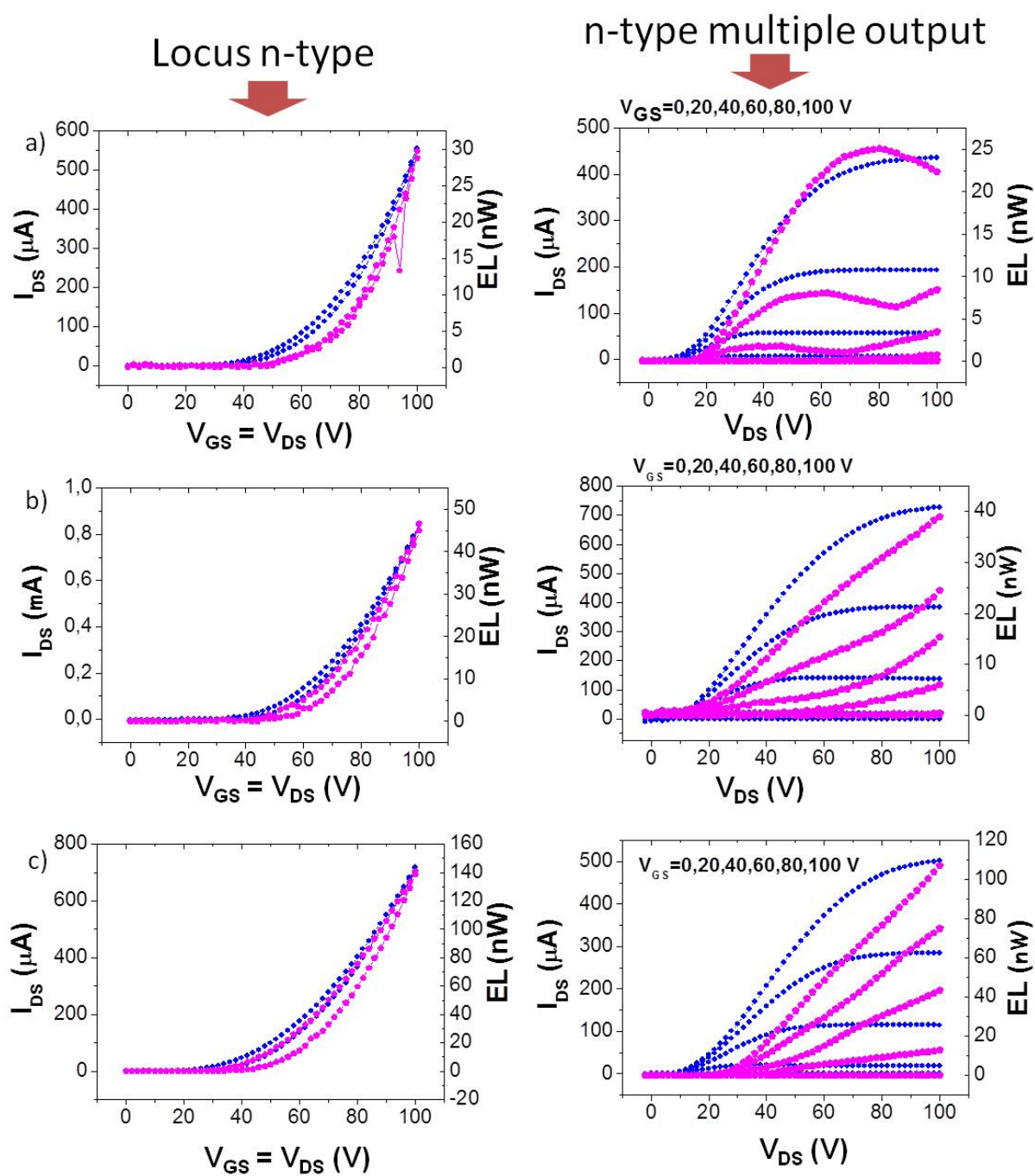

Fig. S8. Electrical responses for compounds C3-NT4N (a), C4-NT4N (b), C6-NT4N (c).

1.8 Computational Details

Density functional theory (DFT) calculations were carried out with the CRYSTAL09 package.[4,5] The exchange-correlation contributions to the total energy were treated using the hybrid B3LYP functional[6,7] with 20% of exact Hartree-Fock exchange that has shown a better agreement with experiments in calculated geometries and vibration frequencies than other functionals (e.g. LDA and GGA).[8,9]

The all-electron Gaussian-type basis sets adopted were 6-31(d1) for oxygen,[10] nitrogen[11] and carbon,[12] 31(p1) for hydrogen[10] and 8-6311(d1) for sulphur.[13] The condition for SCF convergence was set to 10^{-7} and 10^{-10} hartree during geometry optimization and frequency calculation, respectively. In the geometry optimization process the threshold for the maximum and the root-mean-square (RMS) forces and the maximum and the RMS atomic displacements on all the atoms have been set to 0.000450 and 0.000300 a.u. and 0.001800 and 0.001200 a.u., respectively.

Long-range dispersion interactions, of primary importance in molecular crystals, are accounted by a post-DFT dispersive contribution, suggested by Grimme,[14] to the computed ab initio total energy and gradients. Such correction has been recently implemented in the CRYSTAL code and has been successfully validated in particular in combination with the B3LYP functional.[15,16] Van der Waals radii and dispersion coefficients C_6 were taken from Table 1 of reference [17].

Vibrational frequencies, within harmonic approximation, were calculated on the optimized molecule geometry by diagonalising the mass-weighed Hessian matrix W_{ij}

$$W_{ij}(\Gamma) = \sum_G \frac{H_{ij}^{0G}}{\sqrt{M_i M_j}} \tag{1}$$

where H_{ij}^{0G} is the Hessian matrix of second derivatives of the electron+nuclear repulsion energy E evaluated at equilibrium, with respect to the displacement coordinates u_i and u_j of atom A in cell 0 and of atom B in cell G, respectively:

$$\sum_G H_{ij}^{0G} = \sum_G \left[\frac{\partial^2 E}{\partial u_i^0 \partial u_j^G} \right]_0, \quad i=1,...,3N; \quad j=1,...,3N \tag{2}$$

The Hessian matrix is obtained by numerical differentiation of analytical first derivatives $v_j = \partial E / \partial u_j$ using a difference quotient or "two point" formula[5,18]

$$h(x) = \frac{[v_j(x+u_i) - v_j(x)]}{u_i} \tag{3}$$

with a step $u_i = 0.001$Å.

The intramolecular reorganization energy λ_i has been evaluated within the adiabatic potential (AP) approach.[,19] according to the following equation:

$$\lambda_i = E_n(n) - E_n(c) + E_c(c) - E_c(n) \tag{4}$$

where the total electronic energy E subscripts and brackets indicate the charge state and the equilibrium geometry of the neutral (n) and charged (c) molecule, respectively.

In Table S2, all the computed values of λ_i are reported.

Molecule	λ_i^h [meV]	λ_i^e [meV]
C1-NT4N	321	328
C3-NT4N	319	333
C4- NT4N	318	337
C6- NT4N	342	351
C8- NT4N	341	350
C6cyc- NT4N	346	366
C6br- NT4N	330	349

Table S2. Calculated intramolecular reorganization energy, λ_i, by adiabatic potential surfaces of the neutral, cation and anion species.

The charge transfer integral τ is evaluated for the nearest neighboring molecules through the diabatic model[20,21]:

$$\tau = \left\langle \Phi_{FO}^{0,site1} | H | \Phi_{FO}^{0,site2} \right\rangle \tag{5}$$

$\Phi_{FO}^{0,site1}$ and $\Phi_{FO}^{0,site2}$ represent the frontier orbitals (i.e. HOMO or LUMO) of isolated molecules 1 and 2, respectively and H is the electronic Hamiltonian for a non-interacting dimer pair. Here, τ has been estimated through the application of Koopmans' theorem in the energy-splitting in dimer (ESID) model[22]. The charge transfer integrals for hole, τ_h, and for electron, τ_e, transport are computed as half the energetic differences between HOMO and HOMO-1 and between LUMO and LUMO+1 energy levels of a molecular dimer, respectively.

We assumed the non-adiabatic hopping model and we computed the transfer rate constants k_{CT} according to the Marcus-Levich-Jortner formulation[23,24]:

$$k_{CT} = \frac{2\pi}{h} \tau^2 \frac{1}{\sqrt{4\pi\lambda_o k_B T}} \sum_{v=0}^{\infty} \left[\exp(-S_{eff}) \frac{S_{eff}^v}{v!} \exp\left(-\frac{\left(\Delta G^0 + \lambda_o + v\omega_{eff}\right)}{4\lambda_o k_B T} \right) \right] \tag{6}$$

Here, $\Delta G°$ is assumed zero for the self-exchange process (i.e. $M^0 + M^c \leftrightarrow M^c + M^0$, for molecule M in neutral and charged states 0 and c, respectively). The quantum description of normal modes is included through an effective frequency ω_{eff} defined by the following equation:

$$\omega_{eff} = \sum_m \omega_m \frac{S_m}{\sum_n S_n} \tag{7}$$

The summation runs over all the vibrational normal modes m of frequencies ω_m, and S_m denotes the Huang–Rhys (HR) factor measuring charge-phonon coupling strength. The latter can be obtained from the dimensionless displacement parameter B_k:

$$S_k = \frac{1}{2} B_k^2 \tag{8}$$

that, in the harmonic approximation, is defined as:

$$B_k = \sqrt{\frac{\omega_k}{\hbar}} \{X_q - X_p\} M^{0.5} L_k(q) \tag{9}$$

where X_q and X_p are the equilibrium Cartesian coordinates of the q and p charge states, respectively, M is the 3N×3N diagonal matrix of the atomic masses, and $L_k(q)$ is the 3N vector describing the normal coordinate Q_k of the q charge state in terms of mass-weighted Cartesian coordinates.

From Eq (7) the effective Huang-Rhys factor S_{eff} is derived:

$$S_{eff} = \frac{\lambda_i}{\hbar\omega_{eff}} \tag{10}$$

The outer-sphere reorganization energy λ_o in Eq. (10) has been taken as a parameter equal to 0.1 eV, in agreement with recent studies. The bulk charge mobility has been computed assuming a Brownian motion of the charge carrier, described by the following diffusion coefficient D:

$$D = \frac{1}{6} \sum_n (r_n)^2 k_{CT,n} P_n \tag{11}$$

where n runs over all the possible hopping pathways (v. Table 5) and P_n is the probability associated with the hopping defined as follows:

$$P_n = \frac{k_{CT,n}}{\sum_j k_{CT,j}} \tag{12}$$

Finally the bulk charge mobility μ is obtained from the Einstein equation:

$$\mu = \frac{eD}{k_B T} \tag{13}$$

All the calculated charge transport data for molecule C3-NT4N are reported in Table S3.

	ω_{eff} [cm^{-1}]	S_{eff}	μ_{calc} [cm^{2}V^{-1}s^{-1}]	μ_{FET} [cm^{2}V^{-1}s^{-1}]
Hole	968	2.19	1.15 x10^{-1}	1.5x10^{-4}
Electron	978	2.26	1.82 x10^{-1}	2.4x10^{-1}

Table S3. Charge transport data for molecule C3-NT4N: effective frequency ω_{eff} and associated HR factor S_{eff}, computed bulk mobility μ_{calc} and experimental FET mobility μ_{FET}.

1.9 Brightness measurements for compound C6-NT4N

Brightness measurements have been done for the devices reported in Fig. 8c giving values of about 20 cd/m^2 (Fig. S10). We performed the brightness measurements using the standard OLED procedure, so that by keeping the light source far from the detector, in order to satisfy the point-source requirement at the basis of the brightness physical definition. In particular, the sample was kept at 10 and 20 cm far from the detector. Considering that the highest dimension of emitting OLET area is 1,2 cm, and that the detector surface is 1 cm x 1cm, the point source approximation can be considered satisfied. Moreover, at these distances the detector surface can be approximated with a portion of a sphere surface, so delimiting the solid angle portion used to calculate the brightness value.
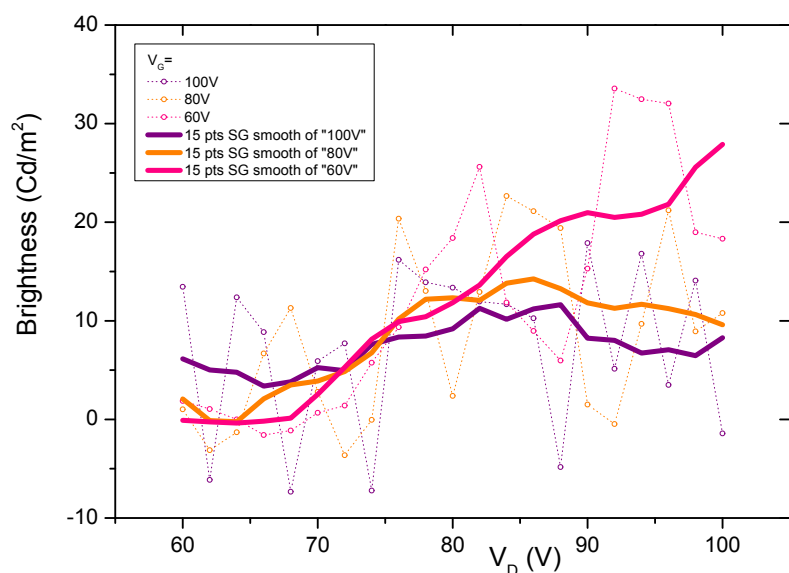

Figure S10. Brightness *vs* drain voltage for compound C6-NT4N at three different gate voltages.

References

[1] Sheldrick, G. *Acta Crystallogr. Sect. A* **2008**, *64*, 112.

[2] Macrae, C. F.; Bruno, I. J.; Chisholm, J. A.; Edgington, P. R.; McCabe, P.; Pidcock, E.; Rodriguez-Monge, L.; Taylor, R.; van de Streek, J.; Wood, P. A. *J. Appl. Crystallogr.* **2008**, *41*, 466.

[3] Macrae, C. F.; Edgington, P. R.; McCabe, P.; Pidcock, E.; Shields, G. P.; Taylor, R.; Towler, M.; van De Streek, J. *J. Appl. Crystallogr.* **2006**, *39*, 453.

[4] R. Dovesi, R. Orlando, B. Civalleri, C. Roetti, V. R. Saunders, C. M. Zicovich-Wilson, *Z. Kristallogr.* **2005**, *220*, 571-573.

[5] R. Dovesi, V. R.; Saunders, C. Roetti, R. Orlando, C. M. Zicovich-Wilson, F. Pascale, B. Civalleri, K. Doll, N. M. Harrison, I. J. Bush, P. D'Arco, M. Llunell, *CRYSTAL09 (CRYSTAL09 User's Manual)*; University of Torino: Torino, **2009**.

[6] A. D. Becke, *J. Chem. Phys.* **1993**, *98*, 5648.

[7] C. Lee, W. Yang, R. G. Parr, *Phys. Rev. B* **1988**, *37*, 785

[8] C. M. Zicovich-Wilson, F. Pascale, C. Roetti, V. R. Saunders, R. Orlando, R. Dovesi, *J. Comput. Chem.* **2004**, *25*, 1873.

[9] S. Tosoni, F. Pascale, P. Ugliengo, R. Orlando, V. R. Saunders, R. Dovesi, *Mol. Phys.* **2005**, *103*, 2549-2558 .

[10] M. Corno, C. Busco, B. Civalleri, P. Ugliengo, *Phys. Chem. Chem. Phys.*, **2006**, 8, 2464.

[11] C. Gatti, V.R. Saunders, C. Roetti, *J. Chem. Phys.*, **1994**, 101, 10686-10696.

[12] M.A. Spackman, A.S. Mitchell, *Phys. Chem. Chem. Phys.*, **2001**, 3, 1518.

[13] V. Maslyuk, C. Tegenkamp, H. Pfnur, T. Bredow, *Chem. Phys. Chem.*, **2006**, 7, 1055.

[14] Grimme, S. *J. Comput. Chem.* **2006**, *27*, 1787–1799.

[15] B. Civalleri, C. M. Zicovich-Wilson, L. Valenzano, P. Ugliengo, *Cryst. Eng. Comm.*, **2008**, *10*, 405-410.

[16] P. Ugliengo, C.M. Zicovich-Wilson, S. Tosoni, B. Civalleri, *J. Mater. Chem.*, **2009**, 19, 2564.

[17] S. Grimme, *J. Comput. Chem*, **2006**, 27, 1787.

[18] F. Pascale, C. M. Zicovich-Wilson, F. L. Gejo, B. Civalleri, R. Orlando, R. Dovesi, *J. Comput. Chem.* **2004**, *25*, 888.

[19] S. Di Motta, E. Di Donato, F. Negri, G. Orlandi, D. Fazzi, C. Castiglioni, *J. Am. Chem. Soc.*, **2009**, 131, 6591.

[20] A. Troisi, G. Orlandi, *Chem. Phys. Lett.*, **2001**, 344, 509.

[21] B. C. Lin, C. P. Cheng, Z. Q. You, C. P. Hsu, *J. Am. Chem. Soc.*, **2005**, 127, 66.

[22] M. Pope, C. E. Swenberg, *Electronic Processes in Organic Crystals and Polymers,* 2nd ed.,

Oxford University Press, New York, **1999**.

[23] R. A. Marcus, *J. Chem. Phys.*, **1956**, 24, 966.

[24] J. Jortner, *J. Chem. Phys.*, **1976**, 64, 4860.